Loquacious-PD facilitates *Drosophila* Dicer-2 cleavage through interactions with the helicase domain and dsRNA

Kyle D. Trettin[a], Niladri K. Sinha[a], Debra M. Eckert[a], Sarah E. Apple[a], and Brenda L. Bass[a,1]

[a]Department of Biochemistry, University of Utah, Salt Lake City, UT 84112

Edited by Rachel Green, Johns Hopkins University, Baltimore, MD, and approved August 13, 2017 (received for review April 27, 2017)

Loquacious-PD (Loqs-PD) is required for biogenesis of many endogenous siRNAs in *Drosophila*. In vitro, Loqs-PD enhances the rate of dsRNA cleavage by Dicer-2 and also enables processing of substrates normally refractory to cleavage. Using purified components, and Loqs-PD truncations, we provide a mechanistic basis for Loqs-PD functions. Our studies indicate that the 22 amino acids at the C terminus of Loqs-PD, including an FDF-like motif, directly interact with the Hel2 subdomain of Dicer-2's helicase domain. This interaction is RNA-independent, but we find that modulation of Dicer-2 cleavage also requires dsRNA binding by Loqs-PD. Furthermore, while the first dsRNA-binding motif of Loqs-PD is dispensable for enhancing cleavage of optimal substrates, it is essential for enhancing cleavage of suboptimal substrates. Finally, our studies define a previously unrecognized Dicer interaction interface and suggest that Loqs-PD is well positioned to recruit substrates into the helicase domain of Dicer-2.

Dicer | RNAi | dsRNA binding protein | protein–protein interaction | endo-siRNA

There are two Dicer genes in *Drosophila melanogaster*, Dcr-1 and Dcr-2, that produce micro-RNAs (miRNAs) and short interfering RNAs (siRNAs), respectively (1, 2). Dcr-2 is required to initiate antiviral RNA interference (RNAi), in which viral double-stranded RNA (dsRNA) is cleaved to produce siRNAs capable of silencing viral gene expression (3, 4). In vitro studies indicate Dcr-2 recognizes dsRNA termini and exhibits termini-dependent cleavage (5, 6). For example, dsRNA with blunt (BLT) termini are cleaved processively in an ATP-dependent manner, while dsRNA with 2-nt 3′overhanging (3′ovr) termini elicit distributive cleavage that occurs in the absence of ATP. Dcr-2's helicase domain plays an important role in termini discrimination (5, 6) and is required to mount an antiviral response (7, 8), suggesting that the termini preferences of Dcr-2 likely arose to distinguish between viral and cellular dsRNA.

Loquacious-PD (Loqs-PD), a dsRNA-binding protein (dsRBP), is required for the biogenesis of a subset of endogenous-siRNAs (endo-siRNAs) (9, 10) but is not required for antiviral RNAi (8). Early studies found that endo-siRNAs map to dsRNA originating from convergent transcription, inverted repeats, and transposons (11–16). Given the sensitive termini dependence of Dcr-2, many endo-siRNA precursors are predicted to be poor substrates. We recently showed that, in vitro, Loqs-PD minimizes the termini dependence of Dcr-2 and facilitates cleavage of suboptimal substrates, including predicted endo-siRNA precursors (6). This suggests Loqs-PD evolved to expand the range of Dcr-2 endogenous substrates; however, the mechanism by which Loqs-PD modulates Dcr-2 substrate recognition and processing is unknown.

Loqs-PD is one of four protein isoforms encoded by the gene loqs. Loqs-PA and Loqs-PB, homologs of TRBP, interact with Dcr-1 during miRNA biogenesis (9, 17–20). Loqs-PC is rarely expressed and has no known function (9). Loqs-PD is the only Loqs isoform capable of facilitating Dcr-2–dependent endo-siRNA biogenesis (19, 20). It contains two dsRNA-binding motifs (dsRBMs) separated by a short linker, with the rest of the protein predicted to be largely unstructured. Only the C-terminal 22 amino acids are unique to the PD isoform (Fig. 1 *A* and *C*), and studies performed in S2 cells indicate they are important for endo-siRNA silencing (21) and for interactions with Dcr-2 (21, 22). However, studies monitoring the interaction between Loqs-PD and Dcr-2 by immunoprecipitation have noted varying degrees of association (9, 10, 23), and so far, studies with purified proteins have not been performed. During RISC assembly, Dcr-2 interacts with another dsRBP, R2D2, and it is unclear whether R2D2 and Loqs-PD compete for the same binding site (23) or bind to unique sites (22).

Using purified components, we performed a series of biochemical experiments to investigate the mechanism by which Loqs-PD modulates Dcr-2 activity. We show that Loqs-PD directly interacts with Dcr-2 in an RNA-independent manner, and this interaction, as well as Loqs-PD binding to dsRNA, are both required for Loqs-PD function. We discovered the first dsRBM of Loqs-PD is uniquely required to enhance cleavage of suboptimal substrates but not an optimal substrate. Finally, we report an unrecognized Dicer–dsRBP interaction interface and describe its potential implication for the function of Loqs-PD.

Results

Purification of Loqs-PD Truncations. We previously showed that Loqs-PD modifies Dcr-2 cleavage activity, but the mechanism by which Loqs-PD accomplishes this is unknown. To identify regions of Loqs-PD required to alter Dcr-2 activity, we designed and purified a series of N- and C-terminal truncations (Fig. 1 *A* and *B*). By precedent (24), each construct was named based on domains or features it contained. For example, the smallest construct, LR_2C, contained the linker region between dsRBMs

Significance

***Drosophila melanogaster* use RNA interference to respond to a viral infection. Dicer-2 cleaves viral double-stranded RNA (dsRNA), producing siRNAs that silence viral gene expression. Dicer-2 recognizes the ends of dsRNA, and this property likely evolved to distinguish between viral and cellular dsRNA. Loquacious-PD (Loqs-PD), a dsRNA binding protein, is not required for Dicer-2's antiviral activity. However, by allowing Dicer-2 to cleave in a termini-independent manner, Loqs-PD facilitates cleavage of endogenous substrates with more complex termini. Our studies are significant because they provide a mechanistic basis for how Loqs-PD modulates Dicer-2 activity. For example, they reveal a previously unrecognized protein–protein interaction interface on the helicase domain of Dicer-2.**

Author contributions: K.D.T. and B.L.B. designed research; K.D.T. and D.M.E. performed research; K.D.T., N.K.S., and S.E.A. contributed new reagents/analytic tools; K.D.T., D.M.E., and B.L.B. analyzed data; and K.D.T. and B.L.B. wrote the paper.

The authors declare no conflict of interest.

This article is a PNAS Direct Submission.

[1]To whom correspondence should be addressed. Email: bbass@biochem.utah.edu.

This article contains supporting information online at www.pnas.org/lookup/suppl/doi:10.1073/pnas.1707063114/-/DCSupplemental.

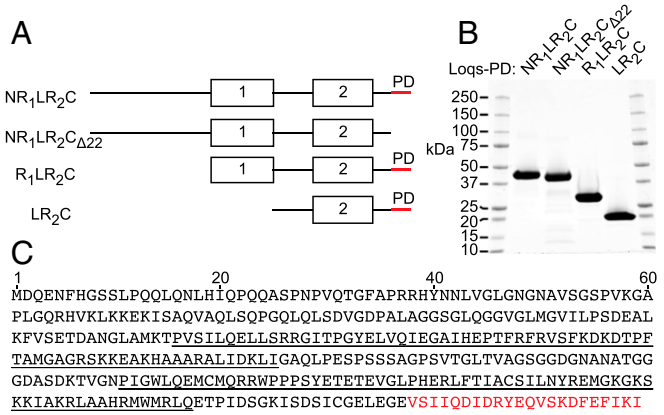

Fig. 1. Design and purification of Loquacious-PD and its truncations. (*A*) Schematic of Loqs-PD and N- and C-terminal truncations. dsRBMs are shown as boxes, and the isoform-specific C terminus is colored red. (*B*) Coomassie-stained SDS/PAGE gel of purified Loqs-PD and truncations. Molecular mass markers were run in first and last lanes with sizes indicated (kDa). (*C*) Primary sequence of Loqs-PD. dsRBMs are underlined, and the 22 C-terminal, isoform-specific amino acids are colored in red.

(L), the second dsRBM (R_2), and the C-terminal tail (C), while the N-terminal region (N) and the first dsRBM (R_1) were deleted. $NR_1LR_2C_{\Delta 22}$ lacked the C-terminal 22 amino acids, which are the only amino acids unique to the PD isoform (Fig. 1*C*). While many dsRBPs form homodimers in solution (25–27), Loqs-PD and all of its truncations were found to be monomers by sedimentation equilibrium experiments (Fig. S1).

Loqs-PD Requires the C-Terminal 22 Residues to Fully Enhance Dcr-2 Cleavage. To determine which domains of Loqs-PD were required to affect Dcr-2 cleavage activity in vitro, we performed single-turnover cleavage assays using dsRNAs with BLT or 3′ovr termini (created by annealing 106-nt sense and antisense RNAs), with $Dcr\text{-}2^{WT}$ alone or supplemented with Loqs-PD or its truncations (Fig. 2 *A* and *B*, Table 1, and Fig. S2). As in our prior studies (6), Dcr-2 alone (-, dotted) cleaved 106 BLT dsRNA at a faster rate (k_{obs}, 0.12 ± 0.02 min^{-1}) than 106 3′ovr dsRNA (k_{obs}, 0.01 ± 0.02 min^{-1}), emphasizing that dsRNA with BLT termini is an optimal substrate compared with dsRNA with 3′ovr, or other non-BLT termini (suboptimal substrates). Inclusion of full-length Loqs-PD (NR_1LR_2C, black lines) dramatically increased the rates of cleavage for both BLT (k_{obs}, 1.98 ± 0.05 min^{-1}) and 3′ovr (k_{obs}, 0.73 ± 0.06 min^{-1}) 106 dsRNA, and a similar rate enhancement was observed when the N-terminal 135 residues were removed (R_1LR_2C, green lines). Conversely, removal of the C-terminal 22 amino acids from Loqs-PD ($NR_1LR_2C_{\Delta 22}$, red lines) severely compromised the ability of Loqs-PD to stimulate Dcr-2 cleavage activity, for both BLT and 3′ovr dsRNA. Thus, the N terminus of Loqs-PD is dispensable for Loqs-PD effects on Dcr-2 cleavage, while the C-terminal 22 amino acids are essential.

Loqs-PD Requires both dsRBMs to Enhance Dcr-2 Cleavage of Suboptimal Substrates. Unexpectedly, additional truncation to remove the first dsRBM (LR_2C, blue lines) revealed substrate-dependent effects. LR_2C increased the Dcr-2 cleavage rate for 106 BLT dsRNA to levels approaching that observed after addition of full-length Loqs-PD (k_{obs}, 1.28 ± 0.07 min^{-1} vs. k_{obs}, 1.98 ± 0.05 min^{-1}). However, while LR_2C slightly increased the Dcr-2 cleavage rate for 106 3′ovr dsRNA, the rate was ∼fourfold slower than that observed in the presence of NR_1LR_2C (k_{obs}, 0.19 ± 0.04 min^{-1} vs. k_{obs}, 0.73 ± 0.06 min^{-1}). To extend these results to a natural, endogenous substrate, we tested a dsRNA derived from *esi-2*, a *Drosophila* endo-siRNA precursor that gives rise to abundant endo-siRNAs in vivo (13–15). *esi-2* contains 20 inverted repeats capable of forming multiple stem-loop, or hairpin, structures, and we used a substrate with a single inverted repeat flanked by noncomplementary sequences. This substrate, referred to as $esi\text{-}2^{hairpin}$ ($esi\text{-}2^{hp}$) [previously referred to as *pre-sl* by Miyoshi et al. (22)], is predicted to form a single hairpin with single-stranded overhangs at each terminus (Fig. 2*D*, *Bottom*). While the endogenous termini of *esi-2* have not been defined, we previously showed that, in vitro, $esi\text{-}2^{hp}$ recapitulates the Loqs-PD–dependent siRNA production (6) observed in vivo (9, 10). We performed single-turnover cleavage assays of $esi\text{-}2^{hp}$ with $Dcr\text{-}2^{WT}$ alone, or supplemented with Loqs-PD or its truncations, in the presence (+) or absence (−) of ATP (Fig. 2 *C* and *D*). Dcr-2 alone was unable to appreciably cleave $esi\text{-}2^{hp}$, while addition of NR_1LR_2C resulted in cleavage and siRNA-sized cleavage products. As with the 3′ovr 106 dsRNA substrate, R_1LR_2C enhanced cleavage of $esi\text{-}2^{hp}$ to the same extent as NR_1LR_2C, while $NR_1LR_2C_{\Delta 22}$ and LR_2C showed a significantly decreased ability to promote cleavage. All cleavage events were dependent on ATP (Fig. 2*C*). Thus, while $esi\text{-}2^{hp}$ differs from 3′ovr 106 dsRNA in that its cleavage is completely dependent on Loqs-PD, it is a suboptimal substrate and, like 3′ovr dsRNA, requires both dsRBMs for cleavage.

In addition to the siRNA-sized cleavage products of $esi\text{-}2^{hp}$, larger products of ∼33 and ∼43 nts accumulated in a Loqs-PD–dependent manner (Fig. 2*C*). In vivo, *esi-2* is processed into two adjacent endo-siRNAs, *esi-2.1* and *esi-2.2*, leaving the ∼42 nt loop region as a byproduct (14) (Fig. S3*A*). To get information about the identity of bands observed in our in vitro cleavage assays, we performed Northern blots in which we probed for a region that encompasses *esi-2.1* (nucleotides 30–60, red), the predominant endo-siRNA observed from *esi-2* (13–15), the loop region (nucleotides 79–109, green), or the 3′ end of $esi\text{-}2^{hp}$ (nucleotides 158–190, blue) (Fig. S3*B*). The "red" probe primarily detected siRNA-sized products, suggesting that siRNA-sized products in Fig. 2*C* include *esi-2.1*. The loop probe primarily detected ∼43 nt-sized products, suggesting the ∼43-nt band in Fig. 2*C* corresponds to the loop region of $esi\text{-}2^{hp}$. Finally, the 3′-end probe detected multiple bands, including likely intermediates, and an ∼33 nt product, suggesting the ∼33-nt band in Fig. 2*C* corresponds to the hairpin base. These data are consistent with cleavage of $esi\text{-}2^{hp}$ to produce two siRNAs and byproducts that include the hairpin loop and base and agree with prior analyses of *esi-2* processing in vivo (14).

Loqs-PD and Its Truncations Bind dsRNA with High Affinity. To gain insight into the differential ability of the Loqs-PD truncations to enhance Dcr-2 cleavage activity, we measured their dsRNA binding affinity. We performed gel mobility shift assays with each Loqs-PD variant and 106 BLT dsRNA (Fig. 3). NR_1LR_2C bound dsRNA with high affinity, exhibiting a K_d of ∼9 nM (Table 1). We observed two faint bands of slower mobility, but the majority of bound or shifted dsRNA appeared as a diffuse smear (Fig. 3*A*, *Top Left*), suggesting a subset of complexes dissociate during electrophoresis (28). $NR_1LR_2C_{\Delta 22}$ bound dsRNA with the same affinity as NR_1LR_2C (K_d of ∼9 nM), and the pattern of shifted dsRNA was also similar (Fig. 3*A*, *Top Right*), indicating deletion of the 22 C-terminal amino acids does not compromise dsRNA binding. R_1LR_2C bound dsRNA with a slightly higher affinity (K_d of ∼1.4 nM) than NR_1LR_2C, suggesting the N-terminal region is inhibitory to dsRNA binding. Further, there was a dramatic change in the pattern of shifted dsRNA. For R_1LR_2C, we observed the sequential appearance of ∼6 distinct complexes (Fig. 3*A*, *Bottom Left*), consistent with a maximal protein to dsRNA stoichiometry of 6:1. In structures with dsRNA, dsRBMs bind ∼16 bp along one face of the dsRNA helix such that another dsRBM can bind opposite the first (29, 30). To accommodate six molecules of R_1LR_2C (∼32 bp) on a 106-bp substrate, we predict binding occurs

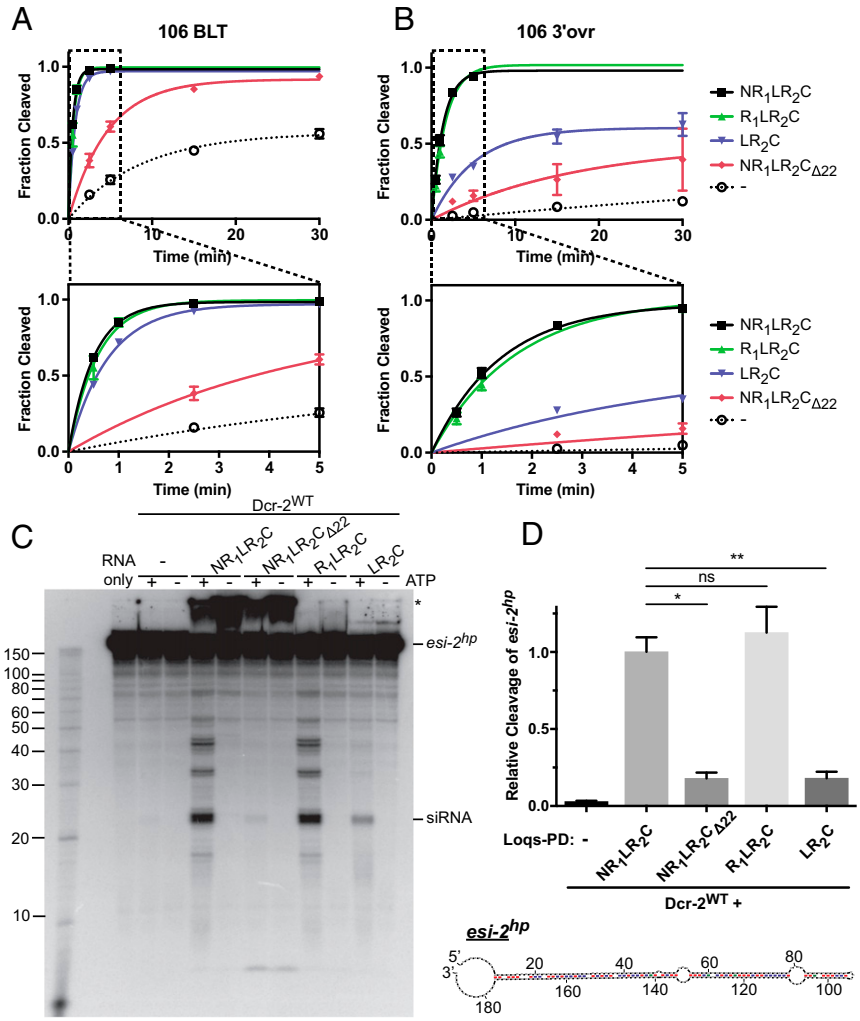

Fig. 2. Loqs-PD truncations affect Dcr-2 cleavage rates in a substrate-dependent manner. Graphs plot single-turnover cleavage over time for 106 BLT (*A*) and 3′ovr (*B*) dsRNA (1 nM) with 30 nM Dcr-2 at 25 °C, in the absence or presence of an equimolar amount of Loqs-PD or its truncations. Portions of *Top* graphs are enlarged below. Data were fit to the pseudofirst order rate equation, $y = y_0 + A \times (1 - e^{-kt})$, where y is fraction cleaved [(cleaved)/(cleaved + uncleaved)], A is amplitude of rate curve (>0.5), y_0 is baseline (=0), k is pseudofirst order rate constant, and t is time. Data points are mean ± SEM (n = 3). (*C*) PhosphorImage shows single-turnover cleavage of ^{32}P-internally labeled *esi-2^{hp}* (1 nM) with Dcr-2 (30 nM), ±Loqs-PD or its truncations (120 nM), ±5 mM ATP. Cleavage products were separated by 12% denaturing PAGE, and 10-nt RNA ladder is on the left. *, RNA trapped in well, possibly due to disordered N terminus of Loqs-PD. (*D*, *Top*) Single-turnover cleavage of *esi-2^{hp}*, with 5 mM ATP and Loqs-PD or truncations, was quantified from data as in *C* (cleavage products divided by total radioactivity in lane) and plotted relative to cleavage with full-length Loqs-PD. Data points are mean ± SEM (n = 3). Paired t test—ns, $P > 0.05$; *$P < 0.02$; **$P < 0.005$. (*D*, *Bottom*) Predicted secondary structure of *esi-2^{hp}* colored according to mFold (58).

along opposite faces of the dsRNA. LR_2C bound dsRNA with slightly lower affinity (K_d of ∼29 nM), consistent with the loss of one of the two dsRBMs. We observed one prominent shift along with a faint second shift. LR_2C also exhibits a Hill coefficient >1, suggesting some form of cooperativity may be operative. As summarized in Fig. 3*B*, removal of the C-terminal 22 amino acids does not alter binding affinity from that of the full-length protein, while removal of the N terminus increases affinity and deletion of both the N terminus and first dsRBM decreases affinity.

The C-Terminal 22 Residues of Loqs-PD Are Necessary for Interaction with Dcr-2. Previous studies suggest the C-terminal 22 residues of Loqs-PD are required to interact with Dcr-2 (21, 22). However, the interaction has not been monitored with purified proteins. Whether Loqs-PD and Dcr-2 interact in the absence of RNA also is untested. To address these questions, we used purified proteins in pull-down experiments with His-tagged Loqs-PD variants and untagged Dcr-2. To facilitate formation of a stable complex, we used a Dcr-2 variant in which both RNaseIII and helicase activity were disrupted by point mutations (Dcr-2^{RIII,K34A}). We

Table 1. Summary of k_{obs}, $t_{1/2}$, and K_d values

	Cleavage of 106 BLT		Cleavage of 106 3′ovr		Binding of 106 BLT	
Loqs-PD	k_{obs}, min^{-1}	$t_{1/2}$, min	k_{obs}, min^{-1}	$t_{1/2}$, min	K_d, nM	h
—	0.12 ± 0.02	5.98	0.01 ± 0.02	66.3	n/a	n/a
NR_1LR_2C	1.98 ± 0.05	0.35	0.73 ± 0.06	0.95	8.97 ± 0.66	1.1 ± 0.1
R_1LR_2C	1.73 ± 0.18	0.40	0.60 ± 0.07	1.16	1.36 ± 0.12	1.8 ± 0.2
$NR_1LR_2C_{\Delta22}$	0.21 ± 0.02	3.25	0.06 ± 0.07	12.0	9.34 ± 0.75	1.1 ± 0.1
LR_2C	1.28 ± 0.07	0.54	0.19 ± 0.04	3.57	29.01 ± 1.3	3.8 ± 0.6
His-LR_2C	1.53 ± 0.06	0.45	n.d.	n.d.	29.93 ± 1.2	3.3 ± 0.4
His-$LR_2C^{K,A}$	0.14 ± 0.01	4.81	n.d.	n.d.	1,631 ± 43	5.0 ± 0.5
His-$LR_2C^{KKK,EAA}$	0.12 ± 0.01	5.62	n.d.	n.d.	1,318 ± 69	3.5 ± 0.5
His-$NR_1LR_2C^{FF,AA}$	n.d.	n.d.	n.d.	n.d.	9.47 ± 1.1	1.0 ± 0.1

Values shown are mean ± SEM (n = 3). n/a, not applicable; n.d., not determined.

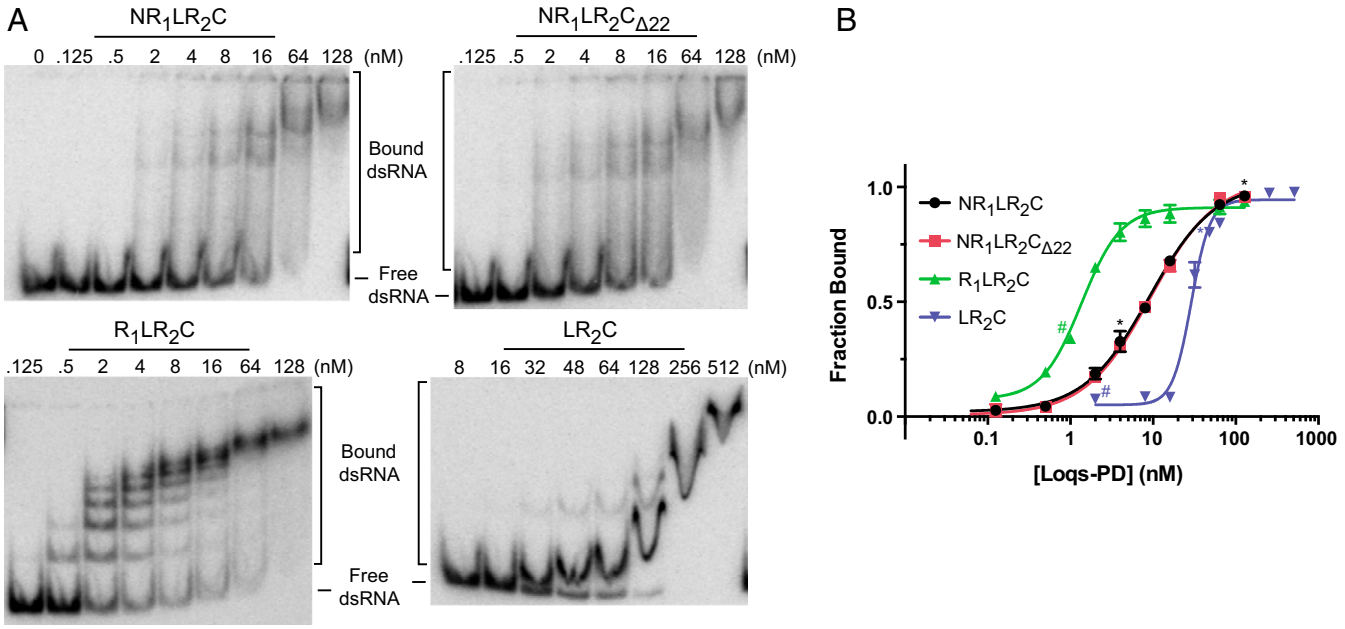

Fig. 3. Loqs-PD and its truncations bind dsRNA with high affinity. (*A*) Representative PhosphorImages for gel shift experiments with 106 BLT dsRNA (10 pM), ^{32}P-end–labeled on the sense strand and incubated with indicated concentrations of Loqs-PD or its truncations. Free dsRNA was separated from bound dsRNA by native PAGE on a 4% 19:1 polyacrylamide gel. (*B*) Radioactivity in gels, as in *A*, was quantified to generate binding isotherms. $dsRNA_{total}$ and $dsRNA_{free}$ were quantified to determine fraction bound ($1 - (dsRNA_{free}/dsRNA_{total})$), and data were fit using the Hill formalism, fraction bound = $1/(1 + (K_d^n/[P]^n))$, where K_d is the dissociation constant, n is the Hill coefficient, and [P] is the protein concentration. Data points are mean ± SEM ($n = 3$ unless marked otherwise; *$n = 2$; #$n = 1$).

found that NR_1LR_2C was able to pull down Dcr-2 (Fig. 4*A*, lane 7), confirming a direct interaction. Additionally, our recombinant proteins were free of RNA as measured by $A_{260/280}$, suggesting this interaction is RNA-independent. By contrast, $NR_1LR_2C_{\Delta 22}$ was unable to pull down Dcr-2 (Fig. 4*A*, lane 8), confirming that the C terminus of Loqs-PD is required for a direct, RNA-independent interaction with Dcr-2. R_1LR_2C and LR_2C were both able to pull down Dcr-2 (Fig. 4*A*, lanes 9 and 10), although R_1LR_2C pulled down slightly less Dcr-2 that NR_1LR_2C or LR_2C (Fig. 4*B*). Thus, Loqs-PD directly binds Dcr-2, and its C-terminal 22 amino acids are required for this interaction.

To determine whether the C-terminal 22 residues of Loqs-PD alone were able to bind Dcr-2, we synthesized the 22-residue peptide (PD22) and performed a competition experiment in which we pulled down Dcr-2 with LR_2C in the presence of increasing amounts of PD22 (Fig. 4 *C* and *D*). PD22 effectively competed for binding with LR_2C as seen by the dose-dependent decrease in the amount of Dcr-2 pulled down by LR_2C (Fig. 4*C*, lanes 9–11 compared with lane 8). To control for nonspecific effects from the high concentration of peptide used, a mutated version of PD22 ($PD22^{mut}$, described below) was tested at the highest concentration of peptide assayed. $PD22^{mut}$ did not compete for the interaction between LR_2C and Dcr-2 (Fig. 4*C*, lane 12), confirming the specificity of the PD22 interaction. We attempted direct binding studies by fluorescence polarization using a fluorescein-labeled version of PD22 but were unable to saturate binding without using prohibitively high concentrations of Dcr-2. Without quantitative binding studies, we cannot rule out that other portions of Loqs-PD contribute to binding, but our analyses indicate the C-terminal 22 amino acids of Loqs-PD directly interact with Dcr-2.

dsRNA Binding Is Required by Loqs-PD to Affect Dcr-2 Cleavage Activity. Our cleavage assays with $NR_1LR_2C_{\Delta 22}$ (Fig. 2) confirmed that the C-terminal 22 residues of Loqs-PD were essential for enhancing Dcr-2 cleavage activity. Our pull-downs (Fig. 4) provided an explanation in that those residues were required for interaction with Dcr-2. An outstanding question was whether dsRNA-binding by Loqs-PD was also required to enhance Dcr-2 cleavage activity. To test this, we disrupted dsRNA-binding activity of Loqs-PD in a construct capable of enhancing Dcr-2 activity. We selected LR_2C because it contained a single dsRBM yet was able to enhance Dcr-2 activity toward a 106 BLT dsRNA to a similar extent as full-length Loqs-PD (Fig. 2*A*). dsRBMs contain a highly conserved KKxxK motif, which mediates direct interaction with the phosphate backbone of dsRNA (29–31). To disrupt the dsRNA-binding activity of LR_2C, we mutated lysine 301, present in the KKxxK motif of dsRBM2 (Fig. 5 *A* and *B*). We performed gel shift assays of 106 BLT dsRNA with His-LR_2C or His-$LR_2C^{K,A}$ (Fig. 5*C*). Indeed, mutation of lysine 301 to alanine resulted in a ~55-fold reduction in binding affinity by His-$LR_2C^{K,A}$ compared with His-LR_2C (Fig. 5*D* and Table 1). The presence of the 6xHis tag had no effect on dsRNA binding (K_d ~ 29 nM vs. K_d ~ 30 nM, respectively) (Table 1). To ensure that the decrease in dsRNA-binding affinity was due to the mutation and not a secondary affect of protein misfolding, we compared His-LR_2C and His-$LR_2C^{K,A}$ by circular dichroism (CD) spectroscopy (Fig. S4*A*). CD spectra reflect the secondary structure composition of a protein (32), and there was no significant difference between the His-LR_2C and His-$LR_2C^{K,A}$ spectra, suggesting the K301A mutation did not grossly affect protein folding. Thus, $LR_2C^{K,A}$ was properly folded but had greatly reduced affinity for dsRNA.

We performed pull-downs with His-$LR_2C^{K,A}$ and found that the dsRBM mutation had no effect on Dcr-2 binding (Fig. 5 *E* and *F*). This result emphasized that the interaction between Dcr-2 and Loqs-PD is independent of dsRNA. After determining that His-$LR_2C^{K,A}$ had greatly reduced dsRNA-binding affinity but was still capable of interacting with Dcr-2, we tested whether His-$LR_2C^{K,A}$ could affect Dcr-2 cleavage activity. We performed single-turnover cleavage assays of 106 BLT dsRNA by $Dcr\text{-}2^{WT}$ alone (−) or supplemented with His-LR_2C or His-$LR_2C^{K,A}$ (Fig. 5*G*). His-$LR_2C^{K,A}$ was unable to increase the rate of Dcr-2 cleavage (Table 1), indicating dsRNA binding is required under

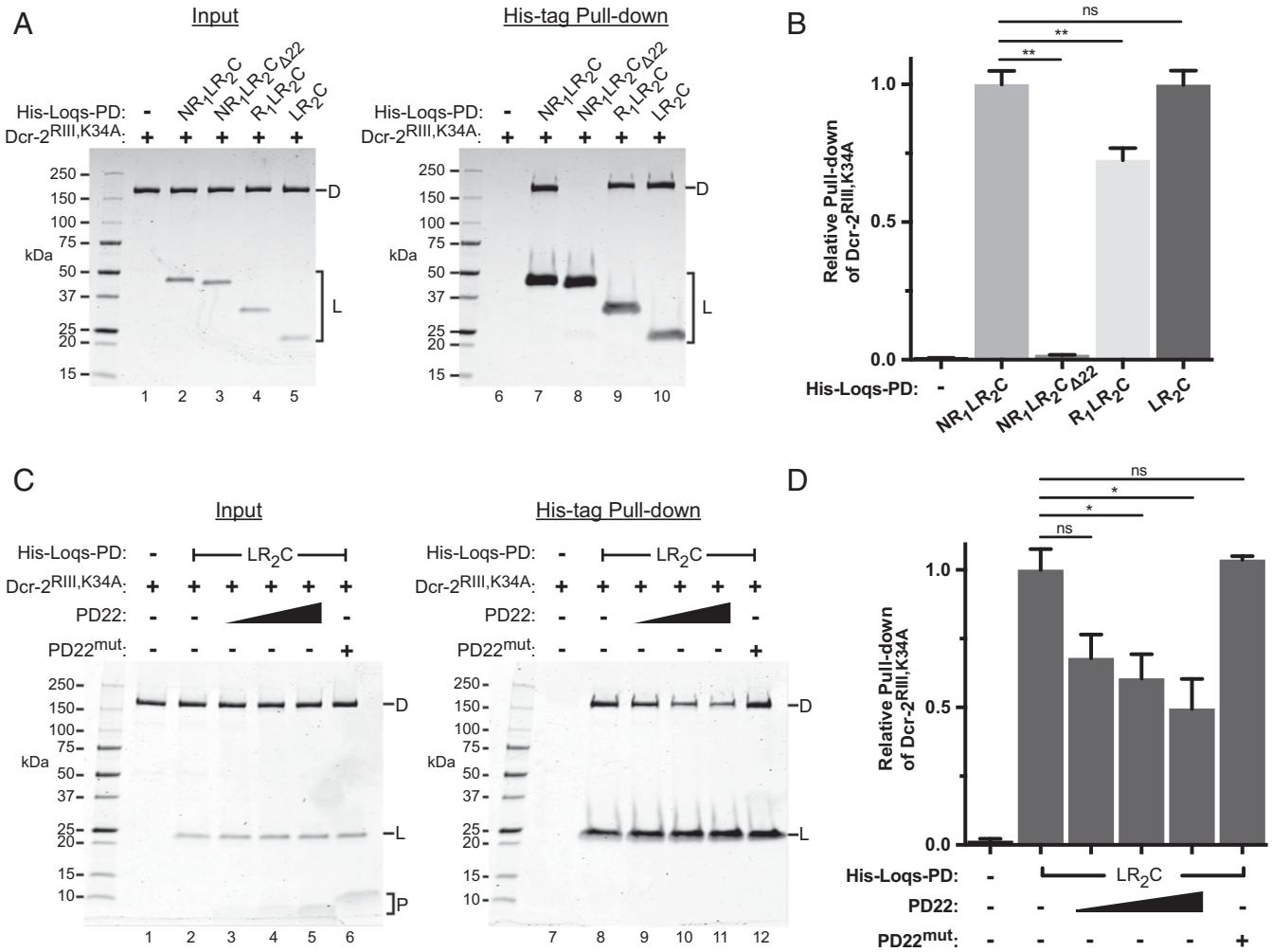

Fig. 4. C-terminal 22 amino acids of Loqs-PD mediate direct interaction with Dcr-2. (*A*) Coomassie-stained SDS/PAGE gels show input (*Left*, 5% of total) and pull-down (*Right*, 100%) of Dcr-$2^{RIII,K34A}$ (D, 2 μM) in the absence (–) or presence of His-tagged Loqs-PD or truncations (L, 4 μM). Molecular mass markers (kDa) are on *Left*. (*B*) Data as in *A* were quantified to determine amount of Dcr-2 pulled down by each Loqs-PD variant. Values were normalized to Dcr-2 in the input and plotted relative to amount pulled down by His–Loqs-PD (His-NR_1LR_2C). Data points are mean ± SEM ($n = 3$); paired *t* test—ns, $P > 0.05$; $^{**}P < 0.003$. (*C*) Pull-down performed as in *A* with increasing amounts of PD22 peptide (P, 10, 20, 40 μM) as a binding competitor. (*D*) Data were quantified as in *B* for pull-downs as in *C*. Data points are mean ± SEM ($n = 3$). Paired *t* test—ns, $P > 0.05$; $^{*}P < 0.04$.

the conditions tested. In addition to the single point mutant, we made a more severe mutant in which all three lysines of the KKxxK motif were mutated to EAxxA (Fig. S4 *B* and *C*). We obtained similar results for K,A and KKK,EAA mutants in all of the above experiments (Table 1 and Fig. S4). Thus, Loqs-PD must bind dsRNA as well as Dcr-2 to enhance Dcr-2 cleavage activity.

Loqs-PD Binds the Hel2 Subdomain of Dcr-2's Helicase. Previous studies indicate Loqs-PD interacts with the helicase domain of Dcr-2 (21), but the exact binding interface is unknown. The helicase domain of Dcr-2 contains two RecA-like domains (Hel1 and Hel2) separated by a Hef-like insertion domain (Hel2i). To identify the region of Dcr-2 that binds Loqs-PD, we coupled protein cross-linking with mass spectrometry (XL–MS), in which hybrid peptides, resulting from intra- or interprotein cross-links, are identified and sequenced by liquid chromatography and tandem MS (LC–MS/MS) (33–35). We performed chemical cross-linking with disuccinimidyl suberate (DSS), a homo-bifunctional NHS-ester cross-linker that primarily reacts with primary amines of lysine side chains or the N terminus (36).

When treated with DSS, Dcr-2 migrated slightly slower during SDS/PAGE (D vs. D+xl) (Fig. 6*A*, compare lanes 1 and 6). Loqs-PD and its truncations migrated slightly faster after DSS treatment, with broader, more diffuse bands (L vs. L+xl; Fig. 6*A*, compare lanes 2–5 and 7–10). In both cases, the altered SDS/PAGE mobility is likely due to intraprotein cross-linking. When Dcr-2 was incubated with NR_1LR_2C and treated with DSS, the main Dcr-2 band (D+xl) shifted to a higher molecular mass species, suggesting formation of a covalent adduct between Loqs-PD and Dcr-2 (D+L+xl) (Fig. 6*A*, compare lanes 6 and 11). Consistent with the requirement of the C-terminal 22 amino acids for interacting with Dcr-2 in pull-down assays (Fig. 4 *A* and *B*), the D+L+xl species was greatly reduced when cross-linking was performed with $NR_1LR_2C_{\Delta 22}$ (Fig. 6*A*, compare lanes 11 and 12). Cross-linking performed with Dcr-2 and R_1LR_2C or LR_2C also resulted in the D+L+xl species (Fig. 6*A*, lanes 13 and 14). The agreement between our cross-linking and pull-downs suggests DSS cross-linking captures the native interaction between Loqs-PD and Dcr-2.

To identify the sites of cross-linking between Dcr-2 and Loqs-PD, we analyzed the in-gel tryptic digest of the D+L+xl species by LC–MS/MS. We identified peptides mapping to both Dcr-2

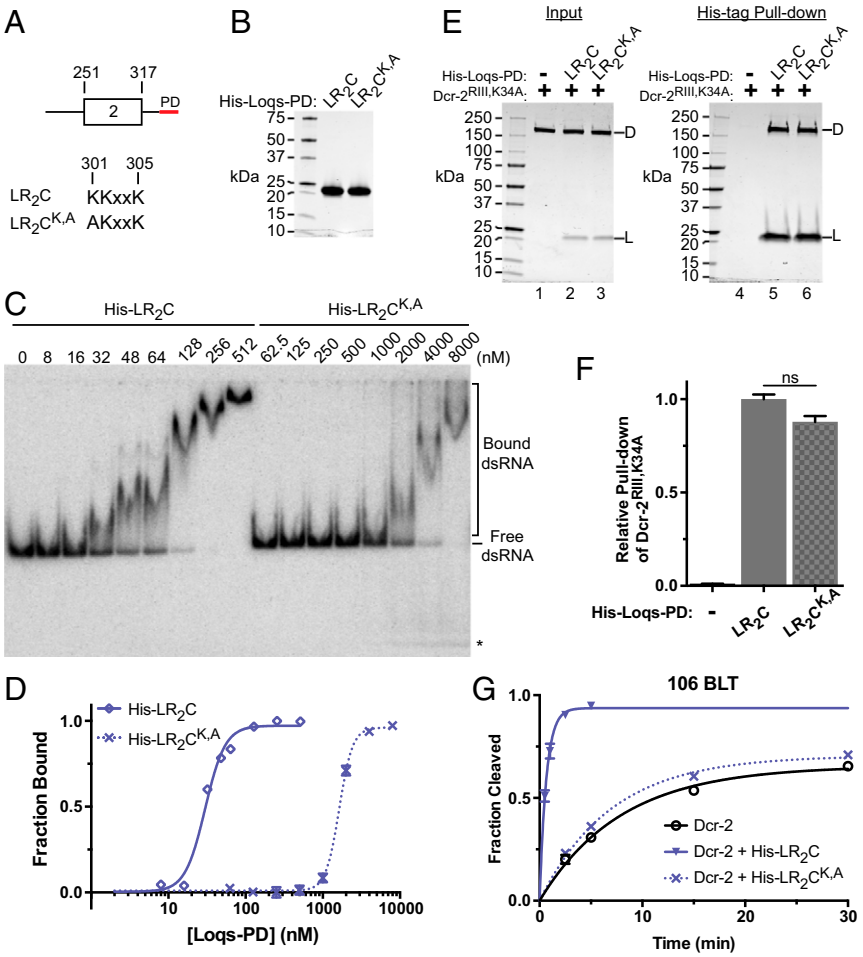

Fig. 5. dsRNA binding is required for LR_2C to affect Dcr-2 cleavage of an optimal substrate. (*A*) Schematic of LR_2C construct and location of mutation to disrupt dsRNA binding. (*B*) Coomassie-stained SDS/PAGE gel of purified His-LR_2C and His-$LR_2C^{K,A}$ with molecular mass markers on the left. (*C*) PhosphorImage of gel shift assay for 106 BLT dsRNA (10 pM), ^{32}P-end–labeled on the sense strand and incubated with indicated concentrations of His-LR_2C or His-$LR_2C^{K,A}$. Free dsRNA was separated from bound dsRNA by native PAGE on a 4% 19:1 polyacrylamide gel. *, trace amounts of ssRNA present with high concentrations of His-$LR_2C^{K,A}$. (*D*) Radioactivity in gels, as in *C*, was quantified to generate binding isotherms as in Fig. 3*B*. Data points are mean ± SEM ($n = 3$). (*E*) Coomassie-stained SDS/PAGE gels show input (*Left*, 5% of total) and pull-down (*Right*, 100%) using Dcr-2^{RIII,K34A} (2 μM) with His-tagged Loqs-PD constructs (4 μM). Molecular mass markers are to the left. (*F*) Quantification as in Fig. 4*B* was performed for data as in *E* and plotted relative to LR_2C. Data points are mean ± SEM ($n = 3$). Paired *t* test—ns, $P > 0.05$. (*G*) Graphs as in Fig. 2*A* show single-turnover cleavage over time for 106 BLT dsRNA (1 nM) with Dcr-2 (30 nM), in the absence or presence, of an equimolar amount of wild-type or mutant His-LR_2C (30 nM). Data points are mean ± SEM ($n = 3$).

and Loqs-PD (Table S1), suggesting the second shift we observed by SDS/PAGE was indeed due to Loqs-PD cross-linking to Dcr-2. We identified 18 Dcr-2–Dcr-2 cross-links and one Dcr-2–Loqs-PD cross-link from two replicates (Fig. 6*B* and Table S2). The sole Loqs-PD–Dcr-2 cross-link and 11/18 Dcr-2–Dcr-2 cross-links were identified in both replicates. We predict all identified Dcr-2–Dcr-2 cross-linked peptides reflect intraprotein rather than interprotein cross-linking because the difference in SDS/PAGE mobility between untreated (D) and treated (D+xl and D+L+xl) samples was very slight. In samples treated with DSS, some protein remained trapped in the wells and may correspond to Dcr-2–Dcr-2 interprotein cross-links that were too large to enter the gel. The sole interprotein cross-link was between the penultimate residue of Loqs-PD, K358, and K501 in Dcr-2, which is located in the Hel2 subdomain of the helicase domain. As a control, we analyzed the in-gel tryptic digest of the D+xl species by LC–MS/MS and identified 16 Dcr-2–Dcr-2 cross-links, and no cross-linked peptides corresponding to Loqs-PD, in two replicates. Nine of 16 Dcr-2–Dcr-2 cross-links were identified in both replicates. Given that the Loqs-PD–Dcr-2 cross-link occurs in the C-terminal 22 residues of Loqs-PD, which are required for interaction with Dcr-2, we predict the reciprocal site of cross-linking in Dcr-2 correctly identifies the interaction surface, Hel2.

Loqs-PD Interacts with Dcr-2 Through an FDF-Like Motif. DSS contains an eight-carbon linker (11.4 Å) between reactive NHS-ester moieties. When cross-linking occurs between lysine side chains, the alpha carbons of each lysine should be within ~24 Å [Lys1 (6.4 Å)–DSS(11.4 Å)–Lys2(6.4 Å)] (37). To verify the specificity of cross-linking, we determined how many of the identified cross-links met this distance constraint. Since the only identified interprotein cross-link to Loqs-PD was in the helicase domain of Dcr-2, we focused analyses on the helicase domain. There are no high-resolution structures available for a Dicer helicase domain, but there are structures available for related helicases from the RIG-I–like and DEAD-box families. We generated a homology model of Dcr-2's helicase domain using Robetta (38) (robetta.bakerlab.org) (Fig. 6*C*). From our combined XL–MS data, we identified seven intraprotein cross-links within the helicase domain. Using our homology model, we measured the distance between alpha carbons of cross-linked residues and found that 7/7 were within 24 Å (Fig. S5*A*); this suggests our homology

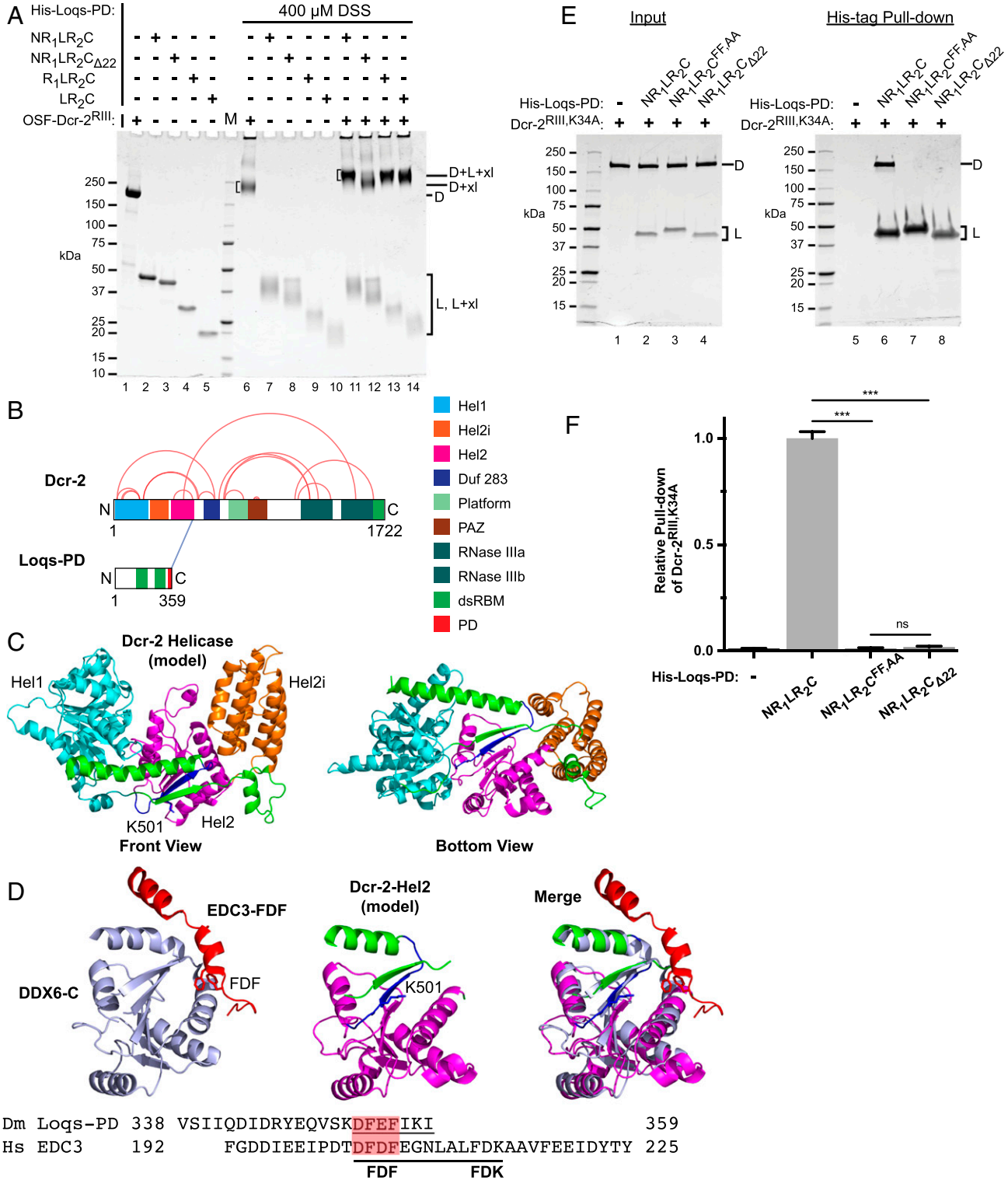

Fig. 6. Loqs-PD interacts with the Hel2 domain of Dcr-2 via an FDF-like motif. (*A*) DSS cross-linking of OSF–Dcr-2^{RIII} (2 μM), in the presence or absence, of Loqs-PD or its truncations (4 μM). Representative Coomassie-stained SDS/PAGE gel of individual proteins without (lanes 1–5, D and L) or with DSS (lanes 6–10, D+xl and L+xl) or together with DSS (lanes 11–14, D+L+xl) ($n > 3$). Brackets mark bands excised for subsequent XL–MS analysis. (*B*) Schematic [xVis (59)] of Dcr-2 and Loqs-PD with color-coded domains depicting intra- and interprotein cross-links identified by MS/MS analysis using ProteinProspector2 (57) in D+L+xl species ($n = 2$). (*C*) Homology model of Dcr-2 helicase domain with Hel1 (cyan), Hel2i (orange), and Hel2 (magenta). The Dcr-2–derived peptide that cross-linked to Loqs-PD is shown (blue), with the site of DSS cross-linking, lysine 501, in stick representation. (*D*, *Top Left*) Complex of DDX6-C (gray) and EDC3-FDF (red). FDF motif is shown in stick representation (PDB ID code 2WAX). (*D*, *Top Middle*) Hel2 from Dcr-2 homology model, colored as in *C*. (*D*, *Top Right*) Structural superposition of DDX6-C:EDC3-FDF complex and homology model of Dcr-2 Hel2 domain. (*D*, *Bottom*) Sequences of *Homo sapiens* EDC3 and C-terminal 22 residues from Loqs-PD. The FDF-motif in EDC3 and the putative FDF-motif in Loqs-PD are shaded in red. (*E*) Coomassie-stained SDS/PAGE gels of input (*Left*, 5% of total) and pull-down (*Right*, 100%) for Dcr-2^{RIII,K34A} (2 μM) with His-tagged Loqs-PD constructs (4 μM). Molecular mass markers are to the left. (*F*) Quantification as in Fig. 4*B* for data as in *E*. Data points are mean ± SEM ($n = 3$). Paired *t* test—ns, $P > 0.05$; ***$P < 0.001$.

model is accurate and that we are detecting structurally plausible cross-links.

We were unable to find documented examples of protein–protein interactions mediated by Hel2 for other RIG-I–like helicases, so we expanded our search to the closely related DEAD-box helicase family (39). DDX6, a DEAD-box helicase involved in mRNA decapping and degradation, interacts with several proteins via its second RecA motif (DDX6-C) (40), which is analogous to Hel2 in Dcr-2. DDX6-C–interacting proteins, such as EDC3, typically bind DDX6 through short peptide interactions involving a Phe–Asp–Phe sequence, known as an FDF motif (40–42) (Fig. 6*D*, *Bottom*). In a crystal structure of DDX6-C and a peptide derived from EDC3 (EDC3-FDF), the two phenylalanines of the FDF motif in EDC3 pack into a hydrophobic pocket on the surface of DDX6-C, distal from the RNA- and ATP-binding sites of DDX6 (43) (Fig. 6*D*, *Left*). Interestingly, Loqs-PD contains a putative FDF-like motif in its C-terminal 22 amino acids (Fig. 6*D*, *Bottom*), raising the possibility that Loqs-PD binds Dcr-2 in a manner analogous to EDC3-FDF and DDX6-C.

We structurally aligned Hel2 of our Dcr-2 helicase model with DDX6-C and noticed that the peptide we identified as cross-linking to Loqs-PD (shown in blue), while not superimposable, was in close proximity to the EDC3-FDF binding site in DDX6-C (Fig. 6*D*, *Right*). To determine if the FDF-like motif of Loqs-PD could bind Dcr-2 similarly to the DDX6-C–EDC3-FDF interaction, we measured the distance between K501 in Dcr-2 and residues in EDC3-FDF that would correspond to K358 of Loqs-PD in either orientation. Both distances were <24 Å, consistent with the distance constraints of DSS cross-linking (Fig. S5*B*). Beyond the FDF-like motif, Loqs-PD and EDC3 have low sequence similarity, and thus, we cannot confidently predict other interactions, or the orientation of Loqs-PD, from the DDX6-C–EDC3-FDF crystal structure.

While additional studies are required to elucidate the detailed interface, our XL–MS data and comparative modeling suggest Loqs-PD interacts with Hel2 of Dcr-2 using a putative FDF-like motif. To directly test this hypothesis, we mutated both phenylalanines in the FDF-like motif of full-length Loqs-PD to alanines (Fig. S6 *A* and *B*). We performed pull-downs of Dcr-2 with His-tagged Loqs-PD constructs, including the FDF-like motif mutant $NR_1LR_2C^{FF,AA}$ (Fig. 6 *E* and *F*). Mutation of the FDF-like motif reduced the interaction between Dcr-2 and $NR_1LR_2C^{FF,AA}$ (compare lanes 6 and 7) to the same extent as deleting the C-terminal 22 residues (compare lanes 7 and 8). This suggests the FDF-like motif in the C-terminal tail of Loqs-PD is required for interaction with Dcr-2. We performed gel shift assays with $NR_1LR_2C^{FF,AA}$ and saw no difference in dsRNA-binding affinity compared with NR_1LR_2C, suggesting that protein folding has not been grossly perturbed (Table 1 and Fig. S6 *C* and *D*). Finally, we compared the ability of the FDF-like motif mutant ($NR_1LR_2C^{FF,AA}$) to promote cleavage of *esi-2*^{hp} to that of either wild-type Loqs-PD (NR_1LR_2C) or the Loqs-PD construct lacking the C-terminal 22 amino acids ($NR_1LR_2C_{\Delta 22}$) (Fig. S6 *E* and *F*). Mutation of the FDF-like motif completely abolished the ability of Loqs-PD to enhance cleavage of *esi-2*^{hp} and is comparable to entirely removing the C-terminal 22 amino acids. Thus, the isoform-specific C terminus of Loqs-PD contains an FDF-like motif that is required for direct interaction with Dcr-2 and to promote cleavage of a suboptimal substrate.

Discussion

Since its discovery, Loqs-PD has been implicated in endo-siRNA biogenesis, but a detailed mechanistic understanding of its function is lacking. Based on our prior study (6) and the biochemical experiments presented here, we propose an integrated model for Loqs-PD function in Dcr-2–dependent siRNA biogenesis (Fig. 7).

In our model, Loqs-PD and Dcr-2 directly interact in the absence of dsRNA (Fig. 7*A*), consistent with our pull-down and cross-linking data (Figs. 4 *A* and *B*, 5 *E* and *F*, and 6*A*). Based on our XL–MS data and subsequent mutational analysis (Fig. 6), the interaction is mediated by an FDF-like motif in the isoform-specific C terminus of Loqs-PD and Hel2 of the Dcr-2 helicase domain. Results from our cleavage assays with $NR_1LR_2C_{\Delta 22}$ (Fig. 2) confirm the necessity of the C-terminal 22 residues for Loqs-PD to fully enhance Dcr-2 cleavage toward both optimal and suboptimal substrates. We predict the defect results solely from an inability of $NR_1LR_2C_{\Delta 22}$ to interact with Dcr-2 (Fig. 4 *A* and *B*) as $NR_1LR_2C_{\Delta 22}$ had unaltered dsRNA binding compared with NR_1LR_2C (Fig. 3). Based on these data, in Fig. 7 we depict the C-terminal 22 amino acids of Loqs-PD, including the FDF-like motif, interacting with Hel2 of Dcr-2 in all conditions and propose it is necessary for Loqs-PD function. Based on our homology model and structures of RNA-bound RIG-I–like helicases (44–48), we predict Loqs-PD is positioned such that it would pull a dsRNA into the C-shaped helicase domain of Dcr-2 (Fig. 7*B*) and that this positioning is critical to its function (see below).

In Fig. 7*C*, we depict the dsRNA–Dcr-2 complex in different conformations for optimal vs. suboptimal substrates, reflecting the intrinsic termini preference of Dcr-2 (6). In the presence of ATP and an optimal substrate (e.g., BLT dsRNA), Dcr-2 is proposed to undergo a conformational change in which the helicase domain clamps onto the dsRNA (closed conformation) to hold it along the body of the enzyme, which in turn promotes processive cleavage (Fig. 7*C*, *Top Left*). For a suboptimal substrate (e.g., 3′ovr or *esi-2*^{hp}) in the presence of ATP, Dcr-2 is proposed to exist predominantly in an open conformation with

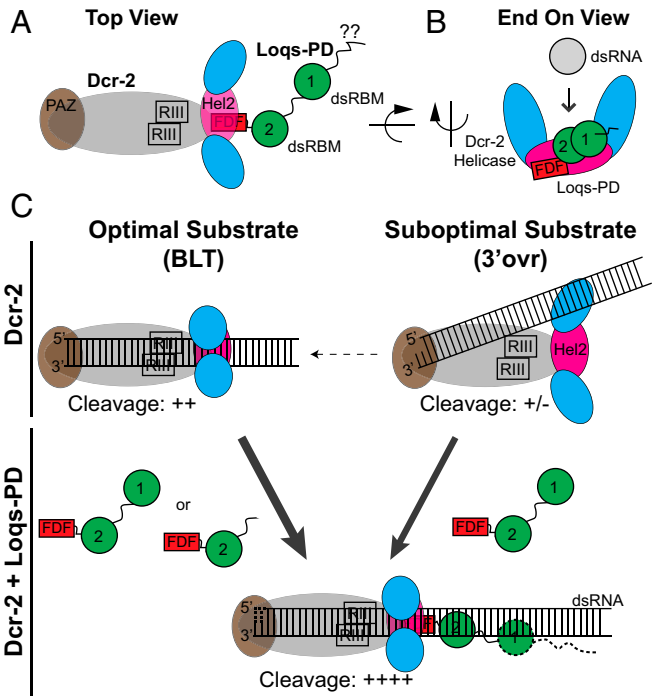

Fig. 7. Model of substrate-dependent requirements for Loqs-PD to affect Dcr-2 cleavage. (*A*) Loqs-PD interacts with Dcr-2 in the absence of nucleotide or dsRNA via the FDF-like motif at the C terminus of Loqs-PD and Hel2 of the Dcr-2 helicase domain. Subdomains of each protein are individually colored and labeled accordingly. (*B*) Interaction with Hel2 positions Loqs-PD at the base of Dcr-2's C-shaped helicase domain. (*C*) Model for termini-dependent Loqs-PD variants dictated by intrinsic termini preference of Dcr-2 in the presence of ATP.

the dsRNA positioned outside of the helicase domain, thus favoring distributive cleavage (Fig. 7*C*, *Top Right*). Based on the experiments reported here, we predict the substrate-dependent conformations of the dsRNA–Dcr-2 complex dictate which domains of Loqs-PD are required to enhance cleavage.

For an optimal substrate, either R_1LR_2C or LR_2C is sufficient to enhance Dcr-2 cleavage (Figs. 2*A* and 7*C*, *Left*). In Fig. 7*C*, *Bottom*, R_1LR_2C/LR_2C is shown interacting with Dcr-2 and the dsRNA substrate, consistent with our findings that dsRNA binding (Fig. 5) and Dcr-2 binding (Figs. 2 and 4 *A* and *B*) are both necessary for Loqs-PD to affect Dcr-2 activity. For an optimal substrate, we predict the dsRNA–Dcr-2 complex is in the closed conformation, which based on crystal structures of RNA-bound RIG-I–like helicases (44–48) would position the dsRNA and Hel2 in close proximity such that LR_2C is sufficient to simultaneously bind both. Thus, we depict LR_2C (highlighted as solid lines in Fig. 7*C*, *Bottom*) holding the dsRNA in the correct orientation relative to the helicase domain to stabilize the closed conformation of the dsRNA–Dcr-2 complex.

For suboptimal substrates, in contrast, R_1LR_2C is the only variant sufficient to fully enhance Dcr-2 cleavage (Figs. 2 *B–D* and 7*C*, *Right*). For a suboptimal substrate, we predict the dsRNA–Dcr-2 complex is predominantly in an open conformation, which based on low-resolution cryo-EM reconstructions of human Dicer bound to an siRNA (49) may position the dsRNA and Hel2 farther apart such that LR_2C is no longer sufficient to simultaneously bind both (Fig. 7*C*, *Top Right*). This model is consistent with our findings that LR_2C interacted with Dcr-2 comparable to full-length Loqs-PD (Fig. 4 *A* and *B*) and bound dsRNA (Fig. 3) yet was not sufficient to fully enhance cleavage of suboptimal substrates (Fig. 2 *B–D*). Given that LR_2C leads to a partial increase in cleavage of suboptimal substrates compared with NR_1LR_2C, we hypothesize that Dcr-2 occasionally transitions into the closed conformation (Fig. 7*C*, dashed arrow) such that LR_2C can stabilize it to promote cleavage. In our model, inclusion of the first dsRBM extends the reach of R_1LR_2C, allowing it to now simultaneously bind both Dcr-2 and the dsRNA substrate. We predict this allows R_1LR_2C to reposition the substrate within the helicase domain of Dcr-2 such that it can now adopt the closed conformation and be stabilized by LR_2C (Fig. 7*C*, *Bottom*). Additional studies are needed to fully elucidate the structures and dynamics of the different conformations discussed.

As a general mechanism, we propose Loqs-PD coordinates Dcr-2 binding with dsRNA binding to promote or stabilize a conformational change in the helicase domain of Dcr-2, which correlates with increased cleavage. Consistent with this model, Loqs-PD has no effect in the absence of ATP (6) (Fig. 2*C*), which we predict is required for the conformational change in Dcr-2. In vivo, under ATP-replete conditions, we expect Loqs-PD directly facilitates endo-siRNA biogenesis by this mechanism, although we cannot rule out the possibility that other factors may further enhance the efficiency.

Many of the annotated Dicer–dsRBP interactions require the helicase domain of Dicer (50, 51), but the exact interface is unknown, with the exception of human TRBP and Dicer. Biochemical and structural studies indicate the third dsRBM of TRBP interacts with Hel2i of Dicer (52, 53). A recent study suggests this interaction is conserved in the fly homologs Dcr-1 and Loqs-PB (20). In contrast, our data indicate that Loqs-PD primarily interacts with Hel2 of Dcr-2's helicase (Fig. 6), identifying an additional Dicer–dsRBP interaction interface. There are conflicting reports as to whether Loqs-PD and R2D2 simultaneously interact with Dcr-2 (22) or whether their binding is mutually exclusive (21, 23). Additional studies are required to determine whether R2D2 binds the same Hel2 interface we have described for Loqs-PD or interacts with Hel2i of Dcr-2 in a manner analogous to TRBP and Dicer. It remains to be seen if other ATP-dependent Dicers such as *Schizosaccharomyces pombe* Dcr1 and *Caenorhabditis elegans* DCR-1 interact with dsRBPs similarly to Dcr-2 and Loqs-PD. Protein–protein interactions mediated by small motifs located in disordered regions have become a dominant theme among RNP assemblies (40, 54).

Materials and Methods

Protein Expression and Purification. Loqs-PD and Dcr-2 were purified from *Escherichia coli* and Sf9 cells, respectively, as described (6) (*SI Materials and Methods*).

Synthesis of PD22 Peptide. PD22 and $PD22^{mut}$ peptides were chemically synthesized as described (55) (*SI Materials and Methods*). Peptide sequences were as follows: PD22: VSIIQDIDRYEQVSKDFEFIKI; $PD22^{mut}$: VSIIQDIDRYEQVSKDAEAIKI.

In Vitro Transcription of RNA Substrates. We prepared 106 dsRNA as described (6). In the plasmid, each RNA strand was flanked by a hammerhead (5′ side) and HDV (3′ side) ribozyme to ensure accurate termini. ^{32}P-end–labeled 106 sense RNA was annealed with 106 BLT or 3′ovr antisense RNA to generate 106 BLT and 106 3′ovr dsRNA, respectively. *esi-2^{hp}* was cloned into the same ribozyme plasmid and prepared as described for 106 dsRNA with minor changes (see *SI Materials and Methods* for details). Sequences of 106 dsRNAs and *esi-2^{hp}* are in *SI Materials and Methods*.

Gel Shift and Cleavage Assays. Gel shift and single-turnover cleavage assays were performed as described (6) with minor changes (see *SI Materials and Methods* for details).

Pull-Down Assays. Dcr-$2^{RIII,K34A}$ (2 μM) and His-Loqs-PD (4 μM) were incubated together in pull-down buffer (25 mM Tris, pH 8, 175 mM KCl, 10 mM $MgCl_2$, 10 mM imidazole, 1 mM TCEP, 5% glycerol, 0.1% nonidet P-40) for 1 h at 4 °C and added to prewashed His-Select Resin (Sigma-Aldrich) for 2 h at 4 °C. Resin and bound proteins were pelleted by centrifugation, and unbound protein (supernatant) was removed. Resin was washed with chilled pull-down buffer, and bound protein was eluted in pull-down buffer containing 300 mM imidazole. Proteins were resolved on a 4–15% gradient gel and stained with Coomassie Brilliant Blue. Competition pull-down assays were performed as described above with addition of PD22 (10, 20, and 40 μM) or $PD22^{mut}$ (40 μM). Bound proteins were resolved on a 4–20% gradient gel by SDS/PAGE.

Chemical Cross-Linking. Dcr-$2^{RIII,K34A}$ or OSF-Dcr-2^{RIII}, and Loqs-PD and its truncations, were dialyzed into cross-linking buffer (20 mM Hepes, pH 7.8, 100 mM KCl, 10 mM $MgCl_2$, 1 mM TCEP, 5% glycerol). Cross-linking reactions were assembled with Dcr-2 (2 μM) and/or Loqs-PD (4 μM) and incubated (25 °C, 30 min). DSS (5 mM in DMSO; Sigma-Aldrich) was added to make 100–400 μM final, and cross-linking was quenched after an additional 30 min at 25 °C with 30 mM Tris, pH 8. Cross-linked proteins were resolved by SDS/PAGE (4–15%) and detected with Coomassie Brilliant Blue.

MS and Identification of Cross-Linked Peptides. Bands corresponding to D+L+xl and D+xl were excised and subjected to in-gel digestion by trypsin and Lys-C. Peptides were extracted, reduced, treated with iodoacetamide, and analyzed using a nano-LC–MS/MS system equipped with a nano-HPLC pump (2D-ultra; Eksigent) and a maXis II ETD mass spectrometer (Bruker Daltonics). The maXis II ETD mass spectrometer was equipped with a captive spray ion source.

Cross-linked peptides were identified using the webserver version of ProteinProspector2 (v5.18.0/1) (prospector.ucsf.edu/prospector/mshome.htm). A custom database was made containing amino acid sequences of Dcr-$2^{RIII,K34A}$ or OSF-Dcr-2^{RIII}, His-Loqs-PD, and 20 decoy proteins. Loqs-PD and Dcr-2 sequences were each randomized 10 times using Decoy Database Builder (56) to generate decoy targets. Up to three missed cleavages were allowed. The MS1 and MS2 mass tolerances were both set to 11 ppm. DSS was specified as the cross-linker. Spectra were annotated as potential cross-linked products if the ProteinProspector total cross-linked product score was >20, and the score difference was >0. To identify high-confidence cross-link products (57), a score difference >8.5 was used, and spectra were manually verified.

Homology Modeling. A homology model of the Dcr-2 helicase domain (residues 1–539) was generated using the Robetta webserver (robetta.bakerlab.org); reference parent structure was DDX3X [Protein Data Bank (PDB) ID code 4PXA].

ACKNOWLEDGMENTS. We thank members of the B.L.B. and Cazalla laboratories for discussion and feedback and Patrick W. Erickson for assistance with CD spectroscopy. Oligonucleotides were synthesized by the DNA/Peptide Facility, part of the Health Sciences Center Cores at the University of Utah. MS was performed at the Mass Spectrometry and Proteomics Core Facility at the University of Utah. MS equipment was obtained through NCRR Shared Instrumentation Grant 1 S10 RR020883-01 and 1 S10 RR025532-01A1. Research reported in this publication was supported by funding from National Institute of General Medical Sciences of the National Institutes of Health Grant R01GM121706 and the H.A. and Edna Benning Presidential Endowed Chair (to B.L.B.) and by funding from National Institute of General Medical Sciences of the NIH Grant P50-GM082545 (to D.M.E.).

1. Lee YS, et al. (2004) Distinct roles for Drosophila Dicer-1 and Dicer-2 in the siRNA/miRNA silencing pathways. *Cell* 117:69–81.
2. Carthew RW, Sontheimer EJ (2009) Origins and mechanisms of miRNAs and siRNAs. *Cell* 136:642–655.
3. Wang X-H, et al. (2006) RNA interference directs innate immunity against viruses in adult Drosophila. *Science* 312:452–454.
4. Sabin LR, et al. (2013) Dicer-2 processes diverse viral RNA species. *PLoS One* 8:e55458.
5. Welker NC, et al. (2011) Dicer's helicase domain discriminates dsRNA termini to promote an altered reaction mode. *Mol Cell* 41:589–599.
6. Sinha NK, Trettin KD, Aruscavage PJ, Bass BL (2015) Drosophila dicer-2 cleavage is mediated by helicase- and dsRNA termini-dependent states that are modulated by loquacious-PD. *Mol Cell* 58:406–417.
7. Deddouche S, et al. (2008) The DExD/H-box helicase Dicer-2 mediates the induction of antiviral activity in Drosophila. *Nat Immunol* 9:1425–1432.
8. Marques JT, et al. (2013) Functional specialization of the small interfering RNA pathway in response to virus infection. *PLoS Pathog* 9:e1003579.
9. Zhou R, et al. (2009) Processing of Drosophila endo-siRNAs depends on a specific loquacious isoform. *RNA* 15:1886–1895.
10. Hartig JV, Esslinger S, Böttcher R, Saito K, Förstemann K (2009) Endo-siRNAs depend on a new isoform of loquacious and target artificially introduced, high-copy sequences. *EMBO J* 28:2932–2944.
11. Ghildiyal M, et al. (2008) Endogenous siRNAs derived from transposons and mRNAs in Drosophila somatic cells. *Science* 320:1077–1081.
12. Watanabe T, et al. (2008) Endogenous siRNAs from naturally formed dsRNAs regulate transcripts in mouse oocytes. *Nature* 453:539–543.
13. Czech B, et al. (2008) An endogenous small interfering RNA pathway in Drosophila. *Nature* 453:798–802.
14. Okamura K, et al. (2008) The Drosophila hairpin RNA pathway generates endogenous short interfering RNAs. *Nature* 453:803–806.
15. Kawamura Y, et al. (2008) Drosophila endogenous small RNAs bind to Argonaute 2 in somatic cells. *Nature* 453:793–797.
16. Chung W-J, Okamura K, Martin R, Lai EC (2008) Endogenous RNA interference provides a somatic defense against Drosophila transposons. *Curr Biol* 18:795–802.
17. Jiang F, et al. (2005) Dicer-1 and R3D1-L catalyze microRNA maturation in Drosophila. *Genes Dev* 19:1674–1679.
18. Saito K, Ishizuka A, Siomi H, Siomi MC (2005) Processing of pre-microRNAs by the Dicer-1-Loquacious complex in Drosophila cells. *PLoS Biol* 3:e235.
19. Fukunaga R, et al. (2012) Dicer partner proteins tune the length of mature miRNAs in flies and mammals. *Cell* 151:533–546.
20. Lim MYT, et al. (2016) The Drosophila Dicer-1 partner loquacious enhances miRNA processing from hairpins with unstable structures at the dicing site. *Cell Rep* 15:1795–1808.
21. Hartig JV, Förstemann K (2011) Loqs-PD and R2D2 define independent pathways for RISC generation in Drosophila. *Nucleic Acids Res* 39:3836–3851.
22. Miyoshi K, Miyoshi T, Hartig JV, Siomi H, Siomi MC (2010) Molecular mechanisms that funnel RNA precursors into endogenous small-interfering RNA and microRNA biogenesis pathways in Drosophila. *RNA* 16:506–515.
23. Marques JT, et al. (2010) Loqs and R2D2 act sequentially in the siRNA pathway in Drosophila. *Nat Struct Mol Biol* 17:24–30.
24. Parker GS, Maity TS, Bass BL (2008) dsRNA binding properties of RDE-4 and TRBP reflect their distinct roles in RNAi. *J Mol Biol* 384:967–979.
25. Cosentino GP, et al. (1995) Double-stranded-RNA-dependent protein kinase and TAR RNA-binding protein form homo- and heterodimers in vivo. *Proc Natl Acad Sci USA* 92:9445–9449.
26. Hitti EG, Sallacz NB, Schoft VK, Jantsch MF (2004) Oligomerization activity of a double-stranded RNA-binding domain. *FEBS Lett* 574:25–30.
27. Parker GS, Eckert DM, Bass BL (2006) RDE-4 preferentially binds long dsRNA and its dimerization is necessary for cleavage of dsRNA to siRNA. *RNA* 12:807–818.
28. Carey J (1991) Gel retardation. *Methods Enzymol* 208:103–117.
29. Ryter JM, Schultz SC (1998) Molecular basis of double-stranded RNA-protein interactions: Structure of a dsRNA-binding domain complexed with dsRNA. *EMBO J* 17:7505–7513.
30. Ramos A, et al. (2000) RNA recognition by a Staufen double-stranded RNA-binding domain. *EMBO J* 19:997–1009.
31. Krovat BC, Jantsch MF (1996) Comparative mutational analysis of the double-stranded RNA binding domains of Xenopus laevis RNA-binding protein A. *J Biol Chem* 271:28112–28119.
32. Provencher SW, Glöckner J (1981) Estimation of globular protein secondary structure from circular dichroism. *Biochemistry* 20:33–37.
33. Holding AN (2015) XL-MS: Protein cross-linking coupled with mass spectrometry. *Methods* 89:54–63.
34. Liu F, Heck AJR (2015) Interrogating the architecture of protein assemblies and protein interaction networks by cross-linking mass spectrometry. *Curr Opin Struct Biol* 35:100–108.
35. Leitner A, Faini M, Stengel F, Aebersold R (2016) Crosslinking and mass spectrometry: An integrated technology to understand the structure and function of molecular machines. *Trends Biochem Sci* 41:20–32.
36. Mädler S, Bich C, Touboul D, Zenobi R (2009) Chemical cross-linking with NHS esters: A systematic study on amino acid reactivities. *J Mass Spectrom* 44:694–706.
37. Merkley ED, et al. (2014) Distance restraints from crosslinking mass spectrometry: Mining a molecular dynamics simulation database to evaluate lysine-lysine distances. *Protein Sci* 23:747–759.
38. Kim DE, Chivian D, Baker D (2004) Protein structure prediction and analysis using the Robetta server. *Nucleic Acids Res* 32:W526–W531.
39. Fairman-Williams ME, Guenther U-P, Jankowsky E (2010) SF1 and SF2 helicases: Family matters. *Curr Opin Struct Biol* 20:313–324.
40. Jonas S, Izaurralde E (2013) The role of disordered protein regions in the assembly of decapping complexes and RNP granules. *Genes Dev* 27:2628–2641.
41. Tritschler F, et al. (2008) Similar modes of interaction enable Trailer Hitch and EDC3 to associate with DCP1 and Me31B in distinct protein complexes. *Mol Cell Biol* 28:6695–6708.
42. Sharif H, et al. (2013) Structural analysis of the yeast Dhh1-Pat1 complex reveals how Dhh1 engages Pat1, Edc3 and RNA in mutually exclusive interactions. *Nucleic Acids Res* 41:8377–8390.
43. Tritschler F, et al. (2009) Structural basis for the mutually exclusive anchoring of P body components EDC3 and Tral to the DEAD box protein DDX6/Me31B. *Mol Cell* 33:661–668.
44. Kowalinski E, et al. (2011) Structural basis for the activation of innate immune pattern-recognition receptor RIG-I by viral RNA. *Cell* 147:423–435.
45. Jiang F, et al. (2011) Structural basis of RNA recognition and activation by innate immune receptor RIG-I. *Nature* 479:423–427.
46. Luo D, et al. (2011) Structural insights into RNA recognition by RIG-I. *Cell* 147:409–422.
47. Wu B, et al. (2013) Structural basis for dsRNA recognition, filament formation, and antiviral signal activation by MDA5. *Cell* 152:276–289.
48. Uchikawa E, et al. (2016) Structural analysis of dsRNA binding to anti-viral pattern recognition receptors LGP2 and MDA5. *Mol Cell* 62:586–602.
49. Taylor DW, et al. (2013) Substrate-specific structural rearrangements of human Dicer. *Nat Struct Mol Biol* 20:662–670.
50. Ota H, et al. (2013) ADAR1 forms a complex with Dicer to promote microRNA processing and RNA-induced gene silencing. *Cell* 153:575–589.
51. Nishida KM, et al. (2013) Roles of R2D2, a cytoplasmic D2 body component, in the endogenous siRNA pathway in Drosophila. *Mol Cell* 49:680–691.
52. Daniels SM, et al. (2009) Characterization of the TRBP domain required for dicer interaction and function in RNA interference. *BMC Mol Biol* 10:38.
53. Wilson RC, et al. (2015) Dicer-TRBP complex formation ensures accurate mammalian microRNA biogenesis. *Mol Cell* 57:397–407.
54. Calabretta S, Richard S (2015) Emerging roles of disordered sequences in RNA-binding proteins. *Trends Biochem Sci* 40:662–672.
55. Petersen ME, Jacobsen MT, Kay MS (2016) Synthesis of tumor necrosis factor α for use as a mirror-image phage display target. *Org Biomol Chem* 14:5298–5303.
56. Reidegeld KA, et al. (2008) An easy-to-use Decoy Database Builder software tool, implementing different decoy strategies for false discovery rate calculation in automated MS/MS protein identifications. *Proteomics* 8:1129–1137.
57. Trnka MJ, Baker PR, Robinson PJJ, Burlingame AL, Chalkley RJ (2014) Matching cross-linked peptide spectra: Only as good as the worse identification. *Mol Cell Proteomics* 13:420–434.
58. Zuker M (2003) Mfold web server for nucleic acid folding and hybridization prediction. *Nucleic Acids Res* 31:3406–3415.
59. Grimm M, Zimniak T, Kahraman A, Herzog F (2015) xVis: A web server for the schematic visualization and interpretation of crosslink-derived spatial restraints. *Nucleic Acids Res* 43:W362–W369.
60. Morse DP (2000) Identification of messenger RNAs that contain inosine. *Methods Enzymol* 318:48–67.
61. Pall GS, Codony-Servat C, Byrne J, Ritchie L, Hamilton A (2007) Carbodiimide-mediated cross-linking of RNA to nylon membranes improves the detection of siRNA, miRNA and piRNA by northern blot. *Nucleic Acids Res* 35:e60.
62. Greenfield NJ (2006) Using circular dichroism spectra to estimate protein secondary structure. *Nat Protoc* 1:2876–2890.
63. Cole JL (2004) Analysis of heterogeneous interactions. *Methods Enzymol* 384:212–232.
64. Laue TM, Shah BD, Ridgeway TM, Pelletier SL (1992) Computer-aided interpretation of analytical sedimentation data for proteins. *Analytical Ultracentrifugation in Biochemistry and Polymer Science*, eds Harding SE, et al. (The Royal Society of Chemistry, Cambridge, UK), pp 90–125.